Extremely Fast Folding of a Very Stable Leucine Zipper with a Strengthened Hydrophobic Core and Lacking Electrostatic Interactions between Helices†

Eberhard Dürr, Ilian Jelesarov, and Hans Rudolf Bosshard*

Biochemisches Institut der Universität Zürich, Winterthurerstrasse 190, CH-8057 Zürich, Switzerland

Received August 6, 1998; Revised Manuscript Received October 20, 1998

ABSTRACT: The dimer interface of a leucine zipper involves hydrophobic as well as electrostatic interactions between the component helices. Here we ask how hydrophobic effects and electrostatic repulsion balance the rate of folding and thermodynamic stability of a designed dimeric leucine zipper formed by the acidic peptide A that contains four repeating sequence units, $(abcdefg)_4$. The aliphatic *a* and *d* residues of peptide A were the same as in the GCN4 leucine zipper but the *e* and *g* positions were occupied by Glu, which prevented folding above pH 6 because of electrostatic repulsion. Leucine zipper A_2 was formed by protonation of the *e* and *g* side chains with a sharp transition midpoint at pH 5.2. Folding could be described by a two-state transition from two unfolded random coil monomers to a coiled coil dimer. There was a linear relationship between the logarithm of the rate constants and the number of repulsive charges on the folded leucine zipper dimer. The same linear relationship applied to the free energy of unfolding and the number of repulsive charges at thermodynamic equilibrium. Fully protonated peptide A folded at a near diffusion-limited rate ($k_{on} = 3 \times 10^8$ M^{-1} s^{-1}), and the free energy of folding was −55 kJ mol^{-1} at 25 °C. The present work shows that protonation of Glu in positions *e* and *g* increases both the folding rate and the stability of the leucine zipper in the absence of any interhelical electrostatic interactions. Protonated Glu is proposed to act like a nonpolar residue and to strengthen the hydrophobic core by folding back toward the core residues in the *a* and *d* positions. This effect adds more to the free energy of unfolding and to the rate of folding than maximizing the number of salt bridges across the helix interface in an electrostatically stabilized heterodimeric leucine zipper [Wendt, H., Leder, L., Härmä, H., Jelesarov, I., Baici, A., and Bosshard, H. R. (1997) *Biochemistry 36*, 204−213].

Coiled coils are helical dimerization motifs found in a wide variety of proteins (*1*). The motif consists of two α-helical peptides wound around each other at an angle of approximately 20° and held together by hydrophobic packing along the dimer interface (*1*−*3*). Each helical peptide chain in isolation is unstable in aqueous solution because the hydrophobic residues are on one face of the helix. This amphipathic structure originates from a seven-residue sequence motif, $(abcdefg)_n$, repeating every two α-helical turns. Hydrophobic residues dominate at the *a* and *d* positions, and Leu, Val, and Ile are particularly frequent. Coiled coils occur as short dimerization motifs in transcription factors known as leucine zippers because leucines are frequent in *d* positions and interdigitate at the dimer interface as in a zipper (*1*, *4*−*6*). Thanks to their repeating sequence pattern coiled coils can be easily designed to study structure−folding relationships (*3*, *7*, *8*).

Hydrophobic packing at the dimer interface is the main force of stabilization of coiled coils. The stability can be controlled additionally by attractive and repulsive electrostatic interactions across the dimer interface (*9*−*18*). The electrostatic effects originate from the close interhelical approach of the side chains in the *e* and *g* positions in the dimer (*9*, *19*, *20*). Natural coiled coils and leucine zippers often have charged residues in the *e* and *g* heptad positions. The contribution of electrostatic attraction between oppositely charged side chains varies with ionic strength and pH. Electrostatic repulsions across the coiled coil interface can strongly oppose folding and thereby control the formation of homo- versus heterodimeric structures (*21*−*23*).

The interface of a coiled coil is formed by residues interacting side-by-side in the *a*, *d*, *e*, and *g* positions as schematically shown in Figure 1. Crystal structures of leucine zippers show apposition of an alkyl side chain in position *d* of one strand to the side chain methylene groups of a charged residue in position *e* of the opposite strand. Similar interactions take place between an alkyl side chain in position *a* and an acidic or basic residue in position *g*. Since the side chains in *e* and *g* are partially exposed to the solvent, they can be charged and at the same time contribute to the hydrophobic nature of the interface.

The kinetics of folding of a leucine zipper are linked to the thermodynamic stability of its coiled coil structure. Only recently have folding kinetics been analyzed (*24*−*29*). Two reaction steps were seen in some cases and have been interpreted as rapid bimolecular association of the unfolded (or partly folded) peptide chains followed by unimolecular rearrangement to the final coiled coil dimer (*24*, *25*, *27*). When folding was very rapid, the reaction was apparently monophasic; that is, folding and association were tightly coupled and could not be resolved in the millisecond time range (*26*−*30*).

Here we extend our investigation on the energetics and kinetics of model leucine zippers by including a structure

† This work was supported in part by the Swiss National Science Foundation (Grant 31.45556.95)

* E-mail: hrboss@bioc.unizh.ch. Fax: +41-1-635 6805.

10.1021/bi981891e CCC: $18.00
Published on Web 12/29/1998

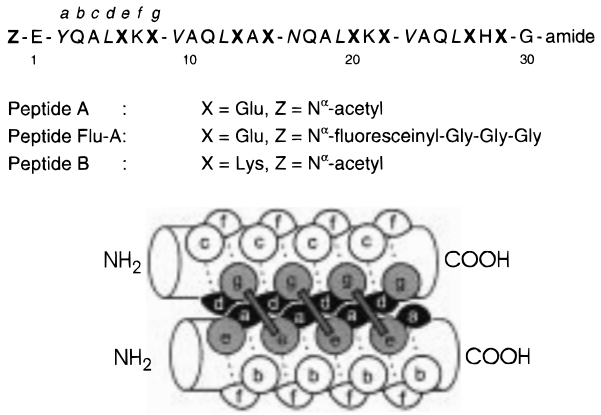

FIGURE 1: Sequence and schematic structure of the parallel two-stranded leucine zippers A_2, $(Flu\text{-}A)_2$, and AB. Sequences: Hydrophobic residues in heptad positions *a* and *d* are in italic; residues in positions *e* and *g* are in bold; and heptads are separated by hyphens. Schematic 3D structure: Each strand of the parallel coiled coil is drawn as a rod with the approximate position of the side chains indicated by spheres. Heptad positions are lettered; positions *a* and *d* are in dark gray; and positions *g* and *e* are in light gray. Interhelical electrostatic interactions between *e* and *g* positions are indicated.

that cannot form interhelical electrostatic bonds. Previously we have studied the heterodimeric model leucine zipper AB composed of an acidic and a basic 30-residue peptide chain. The two chains differ only by having either Glu (peptide A) or Lys (peptide B) in the *e* and *g* positions (Figure 1). Dimer AB is stabilized by interhelical electrostatic bonds (*12*, *16*), which increase the rate of folding but not of unfolding (*29*). Peptides A and B in isolation form homodimeric leucine zippers at low and high pH, respectively, where the repulsive charges are neutralized by protonation/deprotonation [ref *30* and unpublished observation]. We now have studied the energetics and kinetics of folding of acidic peptide A. Specifically, we have addressed the question of how hydrophobic interaction and electrostatic repulsion are balanced across the coiled coil interface to control folding rate and stability. Peptide A folds to the homodimer A_2 when the Glu side chains are progressively protonated. The gradual removal of charge is paralleled by a gradual increase of hydrophobicity because of the weak dipole moment of the protonated glutamic acid side chain. The energetics of folding was studied over a broad temperature range between pH 3 and 6 by CD[1] spectroscopy and DSC. Kinetics of the coupled folding and association reaction were followed by pH jump experiments in the stopped-flow instrument using an N-terminally fluorescein labeled derivative of peptide A whose fluorescence is quenched in the folded dimer (*25*, *27*).

EXPERIMENTAL PROCEDURES

Materials

Peptide Synthesis and Purification. Peptide A and its fluorescein derivative Flu-A were synthesized and purified as described (*30*). Peptide concentrations were determined from UV absorption measurements in 6 M GdmCl, $\epsilon_{275.3} = 1450\ M^{-1}\ cm^{-1}$ (*31*, *32*). Concentration is always expressed as total peptide concentration C_{tot}; for example, 1 μM peptide corresponds to 0.5 μM dimeric coiled coil.

Standard Buffer. Unless indicated otherwise all experiments were conducted in standard buffer of 0.1 M ionic strength. The buffer was composed of 7.5 mM each of phosphoric, citric, and boric acids adjusted to the desired pH with KOH or HCl and to 0.1 M ionic strength with KCl (calculated by program EQUIL, Micromath Inc.).

Methods

Rapid Mixing Experiments. Folding kinetics were studied with an SF-61 stopped-flow spectrofluorimeter (High Tech Scientific Ltd., Salisbury, GB) at 25 °C. The dead time of the instrument was 1−2 ms. Excitation of the fluorescein group of peptide Flu-A was at 485 nm and emission was measured above 530 nm. The instrument time constant was 330 μs for time windows <1 s and 1 ms for time windows >1 s. The results of 6−10 syringe firings were averaged for each kinetic trace. Refolding and unfolding were monitored by rapid dilution of peptide Flu-A into 20 volumes of refolding or unfolding buffer. Refolding jumps were from pH 12 to pH 4.3−5.3 and unfolding jumps from pH 2 to pH 5.2−6. Samples were collected after each mixing reaction to control pH. C_{tot} was 0.25−2 μM for refolding and 0.25−1 μM for unfolding jumps.

Data Analysis of Rapid Mixing Experiments. Refolding and unfolding traces were analyzed for the two-state transition

$$A + A \underset{k_{off}}{\overset{k_{on}}{\rightleftharpoons}} A_2 \tag{1}$$

The fluorescence change during refolding (fluorescence decrease) and unfolding (fluorescence increase) is described by eq 2a and 2b, respectively:

$$F(t) = \Delta F_{max}\left(\frac{[A]}{C_{tot}}\right) + F_{\infty} \tag{2a}$$

$$F(t) = F_0 + \Delta F_{max}\left(1 - \frac{[A]}{C_{tot}}\right) \tag{2b}$$

$F(t)$ is the fluorescence at time t, ΔF_{max} is the maximum fluorescence change, and F_0 and F_∞ are the fluorescence at time zero and at infinite time, respectively. The rate of folding/unfolding is described by

$$-\frac{d[A]}{dt} = k_{on}[A]^2 - 2k_{off}\left(\frac{[C_{tot}] - [A]}{2}\right) \tag{3}$$

where k_{on} and k_{off} are the rate constants of association and dissociation, respectively. The first term on the right of eq 3 is negligible for fast unfolding (pH >5.5), the second term for fast refolding (pH <4.5). Kinetic traces were analyzed by nonlinear curve fitting (program Origin 4.1, MicroCal Software Inc.) with the help of eqs 2a and 2b, respectively, and with [A] defined by the integral of eq 3 (*33*). Results were not affected by the intrinsic change of fluorescence of the fluorescein group with pH since the change occurred within the dead time of mixing.

CD Spectroscopy. CD measurements were performed on a Jasco-715 spectropolarimeter using thermostated cuvettes

[1] Abbreviations: CD, circular dichroism; DSC, differential scanning calorimetry; Flu, fluorescein; GdmCl, guanidinium chloride.

of 1 or 10 mm path length and a bandwidth of 2 nm. Spectra were recorded from 195 to 260 nm at pH values from 2 to 13 and with peptide concentrations from 10 to 350 μM. Data at 222 nm were sampled for 3 min after preincubation for 1 h at a selected pH value. Thermal unfolding curves were obtained by continuously measuring the ellipticity at 222 nm from 5 to 90 °C at a scan rate of 0.8 deg min^{-1} and with data collection every 20 s. Thermal unfolding in the presence of 0−6 M GdmCl was followed from 5 to 55 °C at pH 3.5 after preincubation for at least 1 h. The sample temperature was computer-controlled with an external temperature probe in contact with the water jacket of the cuvette (JULABO F10 circulating water bath). Reversibility of thermal unfolding was checked by two heating and cooling cycles and was better than 95%.

Analysis of CD data. Thermal unfolding curves and pH unfolding curves were analyzed for the two-state transition between unfolded peptide A and folded dimer A_2 described by eq 1. The dissociation/unfolding constant, $K_{unf} = [M]^2/[D]$, is defined by:

$$K_{unf} = \frac{2C_{tot}f_M^{\,2}}{1 - f_M} \tag{4}$$

C_{tot} is the total peptide concentration and f_M the fraction of monomeric peptide A, which can be calculated from

$$f_M = \frac{\sqrt{K_{unf}^{\,2} + 8K_{unf}C_{tot}} - K_d}{4C_{tot}} \tag{4a}$$

The measured molar ellipticity per residue, $[\theta]$, depends on f_M according to

$$[\theta] = f_M([\theta_M] - [\theta_D]) + [\theta_D] \tag{5}$$

$[\theta_M]$ and $[\theta_D]$ are the molar ellipticity per residue of the monomer and the dimer, respectively. $[\theta_D]$ was assumed to depend linearly on temperature and was calculated from $[\theta_D] = [\theta_{D0}] + \alpha T$, where $[\theta_{D0}]$ is the (hypothetical) ellipticity at 0 K and α is a constant. $[\theta_M]$ was independent of temperature. K_{unf} depends on temperature and on the total peptide concentration according to the following (*13, 34*):

$$K_{unf} = C_{tot}\exp\left\{\frac{\Delta H_m}{R}\left(\frac{1}{T_m} - \frac{1}{T}\right) - \frac{\Delta C_p}{RT}\left[T - T_m - T\ln\left(\frac{T}{T_m}\right)\right]\right\} \tag{6}$$

ΔH_m is the enthalpy of unfolding at the transition midpoint temperature T_m ($f_M = 0.5$), ΔC_P is the difference in heat capacity between the unfolded monomeric state and the native dimeric state, and R is the gas constant. CD traces (Figure 5) were analyzed with the help of eqs 4−6 by nonlinear curve fitting and ΔH_m and T_m thus obtained are shown in Table 1. In principle, fitting yields ΔH_m, ΔC_p, T_m, $[\theta_M]$, $[\theta_{D0}]$, and α. Since ΔH_m and ΔC_p are strongly linked, it was not possible to obtain these two parameters by a fit according to eq 6. However, ΔC_p was only about 2 kJ mol^{-1} K^{-1} and, therefore, the second term in the wavy brackets of eq 6 was much smaller than the first and could be neglected in the fitting procedure; that is, ΔC_p was assumed to be 0 for the purpose of the fitting. ΔC_p was obtained afterward from a plot of ΔH_m against T_m (Figure 7).

Thermal unfolding curves were measured in the presence of 0−6 M GdmCl in the range 5−55 °C. Curves from 20 different [GdmCl] were replotted as $[\theta]_{222}$ at constant temperature *versus* [GdmCl]. Values of ΔG^{GdmCl} were calculated from these plots and analyzed by the linear extrapolation method (*35*) according to which $\Delta G^{GdmCl} = \Delta G^{H2O} - m$[GdmCl], where ΔG^{GdmCl} ($= -RT\ln K_{unf}$) is the value measured at a given [GdmCl], and ΔG^{H2O} is the free energy of unfolding (ΔG^{unf}) extrapolated to 0 denaturant concentration (filled circles in Figure 8).

The change of $[\theta]$ with pH (Figure 2) was analyzed by estimating f_M between pH 4.5 and 6 and calculating K_{unf} by using eq 4. The number of protons that are taken up when the coiled coil A_2 is formed at a given pH was calculated from the following (*36*):

$$\Delta\nu = n_{A_2} - 2n_A = \frac{\delta \ln K_{unf}}{\delta \ln [H^+]} \tag{7}$$

n_{A_2} and n_A are the number of protonated glutamic acid side chains in the folded dimer and the unfolded monomer, respectively. The integral $\Delta\nu_{integr}$ in the range pH 2−9 was calculated to get the total number of protons released from A_2 when the pH is raised (Figure 2 inset). $\Delta\nu_{integr}$ is equivalent to the number of negative charges per dimer A_2 (Figures 4 and 9).

Differential Scanning Calorimetry. DSC experiments were performed on the VP-DSC microcalorimeter (MicroCal Inc.) equipped with twin coin-shaped cells of 0.52 mL volume. Technical details and the performance of the instrument have been described (*37*). Peptide A was dialyzed for 18−20 h against the same buffer used to establish the baseline. The scan rate was 1 deg min^{-1}. Reversibility was checked by 2−4 cycles of heating and cooling and was always better than 95%.

Analysis of DSC Data. The unfolding enthalpy was calculated in three different ways. (i) The "true" calorimetric estimate of the unfolding enthalpy was obtained by integration of the area under the excess heat absorption peak. Integration requires knowledge of the temperature dependence of the heat capacities of the folded and unfolded states. Because the transition peak was broad and ΔC_P was small and since the heat capacities before and after the transition were experimentally well-defined and linear, they were connected by a smooth third-order spline function and the peak area above this connection was integrated using the software supplied with the instrument. The values thus obtained are tabulated as ΔH_{cal} in Table 2.

(ii) To test the validity of the two-state model of unfolding accompanied by subunit dissociation and to obtain an additional value of the unfolding enthalpy, we performed a nonlinear regression analysis of the heat capacity traces according to the following equation implemented in the data analysis software of the VP-DSC instrument:

$$C_p = C_p^{\,int} + C_p^{\,ex} = C_p^{\,int} + \frac{\Delta H(T)}{RT^2}\left[\frac{f_M(1 - f_M)}{n - f_M(n - 1)}\right] \tag{8}$$

C_p^{int} is the intrinsic change of heat capacity of the system approximated by a spline function as described above, and

Table 1: Thermodynamic Parameters from Thermal Unfolding Observed by Circular dichroism[a]

pH	C_{tot} (μM)	T_m (K)	ΔH_m (kJ mol^{-1})
5.1	253	318.2	201
5.0	355	327.1	212
4.7	12	317.1	216
	25[b]	321.3[b]	217[b]
	48	323.6	239
	96	325.8	239
	188	330.9	244
	277	334.9	245
	336[c]	335.4	234
	340[c]	334.4	225
	378[c]	335.6	241
4.4	3.12	323.0	231
	6.25[d]	326.5[d]	228[d]
	12.5	328.6	226
	25	332.4	228
	348	342.6	254
4.0	25	339.2	249
	97	346.8	288
	160	349.2	292
	260	352.2	291
3.5	310[c]	357.4	274

[a] Errors of T_m are approximately $\pm$0.25 K and of ΔH_m approximately $\pm$10%. [b] Mean of 4 measurements. [c] Parameters for these peptide concentrations were used to calculate the stability curves shown in Figure 8. [d] Mean of 2 measurements.

n is the number of subunits (peptide chains). f_M can be solved numerically from the following:

$$K = \frac{f_M{}^n n^n A_{tot}{}^{n-1}}{1 - f_M} \quad (9)$$

where A_{tot} is the total concentration of n-mers and K is the equilibrium-unfolding constant of the n-mer given by

$$K = 0.5^{n-1} n^n A_{tot}{}^{n-1} \exp\left[-\frac{\Delta H}{RT}\left(1 - \frac{T}{T_{m0.5}}\right) - \frac{\Delta C_p}{RT}\left(T - T_{m0.5} - T \ln \frac{T}{T_{m0.5}}\right)\right] \quad (10)$$

$T_{m0.5}$ is the temperature at $f_M = 0.5$. Unfolding enthalpies obtained from these fits are shown as ΔH_{fit} in Table 2.

(iii) The effective van't Hoff enthalpy of unfolding (ΔH_{vH} in Table 2) was calculated according to the following (*38*):

$$\Delta H_{vH} = (\sqrt{n} + 1)^2 T_m \sqrt{R\left(\langle \Delta C_p \rangle_{max} - \frac{\Delta C_p \sqrt{n}}{\sqrt{n} + 1}\right)} \quad (11)$$

$\langle C_p \rangle_{max}$ is the heat capacity at T_m, ΔC_p is the unfolding heat capacity increment, and $n = 2$ for a bimolecular transition.

Model Building. A model of folded A_2 with all of its glutamic acid side chains protonated was built with the crystal structure of the 33-residue leucine zipper of transcription factor GCN4 as a template (PDB entry 2zta.pdb; ref 19). Side chains were replaced to correspond to the sequence of peptide A. Steric clashes were removed by selecting suitable rotamers. Atomic parameters were assigned according to the CVFF force field as implemented in the program Discover3 (Biosym/MSI Inc.). The model was minimized in vacuo for 1000 steps using the steepest descents and conjugate gradient algorithms and a distance-dependent dielectric approximation. The minimized structure was soaked in a 30 $\times$ 30 $\times$ 60 Å box containing 2500 water molecules, and a molecular dynamics simulation was performed for 100 ps at 298 K and with 1 fs time steps. Snapshots were collected every 10 ps and were subjected to minimization. ΔC_P was calculated from the following (see Table 13 in ref 39): ΔC_P(J mol^{-1} K^{-1}) = $2.14\Delta A_{al} + 1.55\Delta A_{ar} - 1.27\Delta A_{pol}$ where ΔA_{al}, ΔA_{ar}, and ΔA_{pol} are differences in surface area (in Å^2) composed of aliphatic, aromatic, and polar side chains, respectively, between the fully extended peptide A and the fully protonated coiled coil A_2 modeled on the GCN4 leucine zipper structure. Protonated Glu was treated as a polar side chain.

Table 2: Thermodynamic Parameters Determined by Differential Scanning Calorimetry[a]

pH	C_{tot}	T_m[b] (K)	$T_{m0.5}$[c] (K)	ΔH_{cal}[d] (kJ mol^{-1})	ΔH_{vH}[e] (kJ mol^{-1})	$\Delta H_{cal}/\Delta H_{vH}$	ΔH_{fit}[f] (kJ mol^{-1})
4.7	105	336.1	334.1	230	230	1.00	224
	135	337.8	335.6	231	235	0.98	225
	188	335.0	333.0	209	225	0.93	207
	277	337.4	335.7	215	231	0.93	212
	336[g]	339.5	337.1	225	223	1.01	217
	353[g]	341.0	338.7	235	239	0.98	229
	378[g]	339.7	337.6	203	225	0.90	207
	399[g]	345.0	342.8	228	242	0.94	236
4.4	150	343.7	342.0	223	250	0.89	223
	213	345.3	343.4	231	258	0.90	234
	335	349.9	348.0	247	251	0.98	246
	585	353.3	351.4	245	263	0.93	250
4.0	97	349.5	347.9	237	259	0.92	237
	160	351.9	350.3	239	267	0.89	237
	260	354.5	347.9	242	267	0.91	240
3.5	96	354.9	353.2	252	251	1.00	243
	190	357.9	356.3	265	282	0.94	257
	310[g]	359.3	357.9	269	275	0.98	260
	394[g]	360.7	359.1	256	283	0.91	259

[a] Errors of T_m and $T_{m0.5}$ are approximately $\pm$0.25 K and of ΔH approximately $\pm$10%. [b] Temperature at the maximum of the heat capacity trace. [c] Temperature where the transition was half-completed. Value obtained by fitting according to eq 10. [d] Excess enthalpy calculated by integration of the heat absorption peak after subtraction of a cubic spline function connecting the pre- and post-transition heat capacity trace. [e] Excess enthalpy calculated according to eq 11. [f] Excess enthalpy calculated according to eq 10. [g] Parameters for these peptide concentrations were used to calculate the stability curves shown in Figure 8.

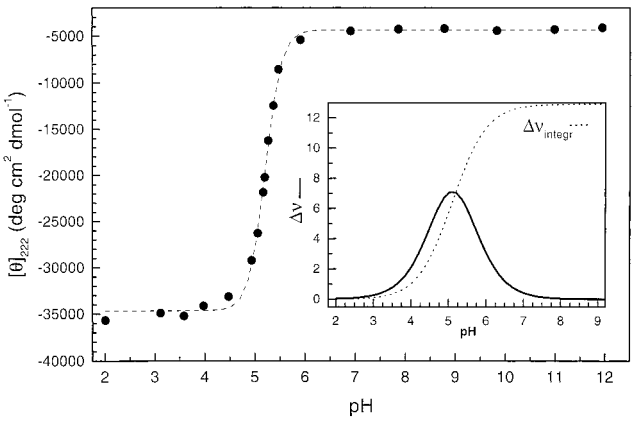

FIGURE 2: Influence of pH on the molar CD absorption per residue at 222 nm of peptide A. Measurements were made with 25 μM peptide. Inset: solid line, $\Delta\nu$ calculated by eq 7; dotted line, integral $\Delta\nu_{integr}$ (area under the solid line). $\Delta\nu$ is the difference in the number of protons between the folded leucine zipper and the unfolded peptide chains at a given pH. The peak of the bell-shaped curve described by $\Delta\nu$ is at pH 5.1, close to the pH midpoint of the titration curve of the main plot. $\Delta\nu_{integr}$ is the total number of negative charges on folded A_2 at a given pH.

RESULTS

Structure of Peptide. The sequence of peptide A is shown in Figure 1. The pattern L^d V^a L^d N^a L^d V^a L^d of hydrophobic residues in positions *a* and *d* was the same as in the natural leucine zipper domain of the yeast transcription factor GCN4 except for Tyr in the first *a*-position which served as a chromophore for the determination of peptide concentration. The central Asn stabilizes a parallel and in-register dimeric coiled coil (*40*−*43*). Helix-stabilizing residues were selected for the solvent-exposed positions *b*, *c*, and *f*. The two Lys and the single His in solvent-exposed *f* positions helped to keep the peptide soluble at low pH. At neutral pH, unfolded peptide A had a calculated net charge of $-7e$. At pH <3, the net charge was $+3e$. The charges in the three solvent-exposed *f* positions were far apart in the coiled coil structure. These positive charges were not taken into account when referring to the number of charges on peptide A or dimer A_2.

Protonation Induces a Dimeric, Parallel Leucine Zipper. The CD spectrum of peptide A at pH 3.0 was typical of an α-helical structure with minima at 208 and 222 nm and with $[\theta]_{222} = -35.000$ deg cm^2 dmol^{-1} accounting for nearly 100% helix content. Above pH 6 the spectrum was typical of a random coil structure (not shown). The protonation-induced spectral change at 222 nm is shown in Figure 2. The transition was very sharp and had a midpoint at pH 5.2.

Previously we had shown that at pH 2 the fully protonated peptide A sediments with an apparent mass of 6530 ± 60 Da, close to the calculated mass of 6936 Da of the dimer A_2 (*30*). This result together with the helical CD spectrum was clear evidence for a dimeric leucine zipper. The two chains were parallel because the fluorescence emission of the derivative Flu-A was strongly quenched, which was only possible in the parallel but not in the antiparallel orientation (*27*, *30*). The parallel orientation was confirmed in the present study by mixing peptide Flu-A at pH 3 with a 2-fold excess of nonfluorescent peptide A. Fluorescence emission increased by 2-fold after mixing, in line with strand exchange between the fluorescent and nonfluorescent parallel coiled coils (not shown).

The fraction of monomeric peptide A, f_M, was extracted from the curve shown in the main part of Figure 2 to calculate K_{unf} by eq 4. K_{unf} was then used to calculate $\Delta\nu$, the number of protons taken up on folding at a given pH. $\Delta\nu$ describes a bell-shaped curve. Its midpoint is at pH 5 where $\Delta\nu = 7$, which means that seven protons are taken up when two peptides A associate and fold to A_2 at pH 5. Integration yields the number of negatively charged Glu side chains on folded A_2, designated as $\Delta\nu_{integr}$. Since unfolded peptide A at high pH has 9 charges, 18 protons have to be taken up to reach the fully protonated A_2, but only 13 protons are involved in the folding process between pH 9 and 2 (dotted line in Figure 2 inset). This indicates that the folded dimer does not appear before on average 5 glutamate side chains are already protonated.

Kinetics of the Coupled Association and Folding Reaction. The kinetics of folding were measured with the help of the fluorescein-labeled peptide Flu-A (Figure 1). Fluorescence emission of the fluorescein group attached to the N- or C-terminus of a coiled coil is quenched in the folded coiled coil by self-quenching (*25*, *27*). The fluorescein group does not interfere with folding since it is separated from the coiled coil by a three-residue spacer (*25*, *27*). Refolding and unfolding were followed by rapid jumps from pH 12 to pH 4.3−5.3 and from pH 2 to pH 5.2−6, respectively. Kinetic traces were well-described by eq 3 for a two-state transition between two unfolded monomers and a folded dimer (Figure 3). The rate of folding was proportional to the peptide concentration, indicating that folding was limited by a reaction that required monomer−monomer collision. Unfolding was independent of peptide concentration. Plots of ln k_{on} and ln k_{off} against $\Delta\nu_{integr}$, the number of negative charges on A_2, are shown in Figure 4. k_{on} increased and k_{off} decreased when peptide A was gradually protonated. The change of ln k_{on} and ln k_{off} with $\Delta\nu_{integr}$ is linear and can be described by the following equations:

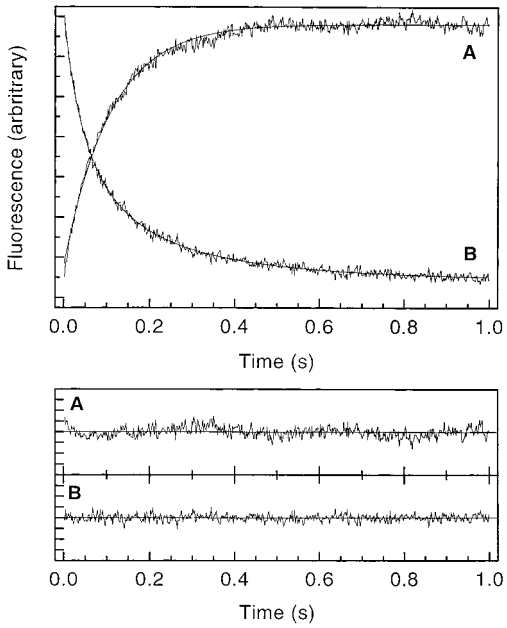

FIGURE 3: Examples of fluorescence stopped-flow experiments: trace A, unfolding jump from pH 2 to 5; trace B, refolding jump from pH 12 to 4.9. Solid lines are best fits described by eq 3 for folding (eq 2a) and unfolding (eq 2b), respectively. Total peptide concentration after mixing was 1 μM. Residuals of the fits are shown in the lower panels. The wavy shape of the residual for trace A is an instrument artifact.

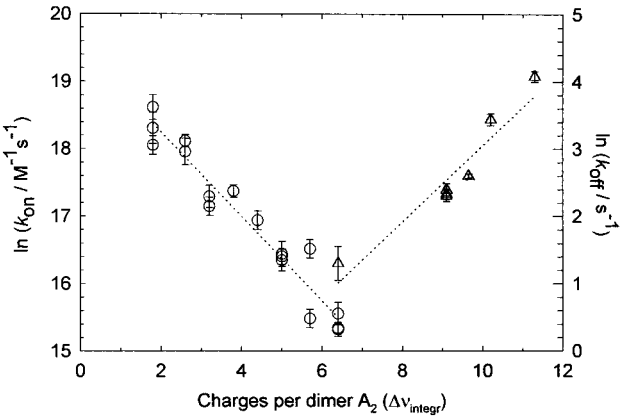

FIGURE 4: Change of ln(k_{on}) (circles) and ln(k_{off}) (triangles) with $\Delta\nu_{integr}$, the number of negative charges on A_2. The dotted lines are best fits (eq 12) for $k_{on}^0 = 3 \times 10^8$ M^{-1} s^{-1}, $k_{off}^0 = 7.2 \times 10^{-2}$ s^{-1}, $m_{on} = -0.63$ charge^{-1}, and $m_{off} = 0.57$ charge^{-1},

$$\ln(k_{on}) = \ln(k_{on}{}^0) + m_{on}\Delta\nu_{integer} \quad (12)$$

$$\ln(k_{off}) = \ln(k_{off}{}^0) + m_{off}\Delta\nu_{integer}$$

where the superscript 0 indicates $\Delta\nu_{integr} = 0$ and m_{on} and m_{off} are the slopes of the dotted lines in Figure 4. Because we find $|m_{on}| \approx |m_{off}|$, folding and unfolding rates were controlled to the same extent by the number of negative charges on A_2. Extrapolation to fully protonated A_2 yields $k_{on}{}^0 = 3 \times 10^8$ M^{-1} s^{-1} and $k_{off}{}^0 = 7.2 \times 10^{-2}$ s^{-1}. These are the rate constants of folding and unfolding for two fully protonated peptides in equilibrium with the coiled coil conformation.

For a two-state folding reaction the free energy of unfolding and dissociation of A_2, ΔG^{unf}, can be expressed as

$$\Delta G^{unf} = -RT \ln\left(\frac{2k_{off}}{k_{on}}\right) \quad (13)$$

Combining eqs 12 and 13 gives:

$$\Delta G^{unf} = -RT \ln\left(\frac{2k_{off}{}^0}{k_{on}{}^0}\right) - RT(m_{off} - m_{on})\Delta\nu_{integr} \quad (14)$$

By using eq 14 and $\Delta\nu_{integr}$(pH) shown in the inset of Figure 2, one calculates ΔG^{unf}(25 °C) = 52 kJ mol^{-1} at pH 3.5 and ΔG^{unf}(25 °C) = 41.8 kJ mol^{-1} at pH 4.7. These values are in very good agreement with the values obtained by equilibrium thermodynamics: ΔG^{unf}(25 °C) = 55 kJ mol^{-1} at pH 3.5 and ΔG^{unf}(25 °C) = 42.5 kJ mol^{-1} at pH 4.7 (see below and Figure 8).

Thermal Denaturation Followed by CD. The CD spectra of peptide A in the range 10−70 °C and at pH 4.7 showed a typical transition from helical to random coil with an isodichroic point at 203 nm, indicative of a two-state transition (not shown). The same isodichroic point was observed for thermal unfolding of heterodimeric leucine zipper AB (*16*) and for salt-induced folding of peptide A (*30*). Thermal unfolding was followed between pH 5.1 and 2 and for peptide concentrations in the range 10−400 μM. Unfolding was reversible at all pH values. The midpoint temperature of transition, T_m, depended on pH and concentration. The entire set of T_m values covered a range of 44 degrees. Values of T_m and ΔH_m calculated for a two-state transition model are summarized in Table 1. Figure 5 shows examples of CD unfolding curves at different pH and peptide concentrations.

Thermal Denaturation Followed by DSC. Calorimetric experiments were performed in the range pH 2−5.1 and with C_{tot} between 100 and 400 μM. Thermal unfolding was >95% reversible over three consecutive cycles of heating and cooling. To probe for heat effects caused by buffer protonation, we repeated experiments in 7.5 mM acetate buffer adjusted to 0.1 M ionic strength. Results were identical to those obtained in the standard buffer verifying that the measured enthalpy change was the true unfolding enthalpy. Representative traces are shown in Figure 6. At pH <3, the post-transitional heat capacity tended to drop slightly, a possible sign of aggregation of the unfolded peptide. At pH >4.9, the pre-transitional heat capacity trace was very steep

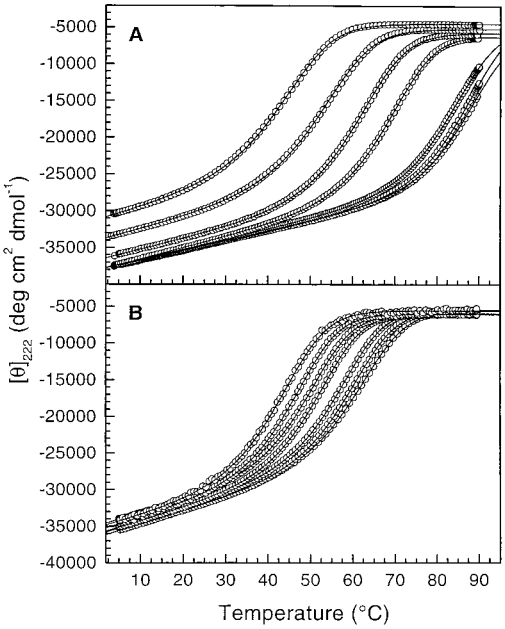

FIGURE 5: CD thermal melting curves. (A) Melting at pH 5.1, 5.0, 4.7, 4.5, 3.5, 3.0, and 2.0 (left to right). (B) Melting at pH 4.7 for 12, 25, 48, 96, 188, 277, and 378 μM peptide (left to right). Solid lines are best fits according to eqs 4−6 for the two-state folding model A + A ⇌ A_2.

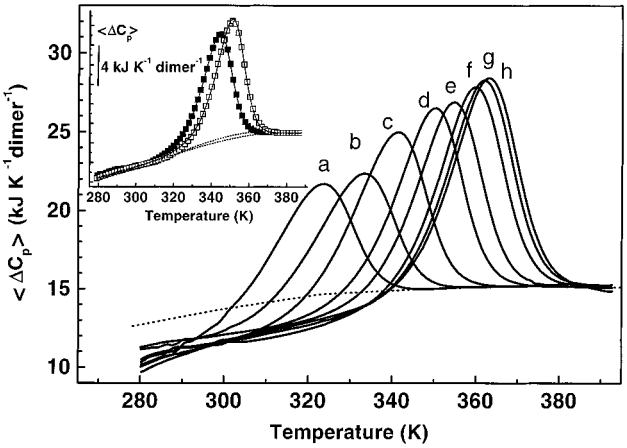

FIGURE 6: Partial molar heat capacity of peptide A. DSC traces labeled a−h were obtained at the following conditions of pH and total peptide concentration: a, pH 5.1 and 253 μM; b, pH 4.9 and 355 μM; c, pH 4.7 and 353 μM; d, pH 4.4 and 335 μM; e, pH 4.0 and 260 μM; f, pH 3.5 and 310 μM; g, pH 3.0 and 292 μM; h, pH 2.5 and 331 μM. The dotted line indicates the partial molar heat capacity of the denatured state calculated from the amino acid composition of peptide A (*72*). Traces are shifted on the *y*-axis to fit to the calculated C_p of the unfolded state. Experiments were performed in standard buffer except for trace e which was made in 7.5 mM acetate buffer. (inset) Representative examples of fitting the DSC data to a two-state unfolding transition accompanied by dissociation according to eq 8: filled symbols, fit to trace c of main figure; open symbols, fit to trace d of main figure; dotted lines, intrinsic change of C_p (of the system) approximated as described in Methods.

indicating that transition started at low temperature and peptide A was not fully folded even below 20 °C. The transition heat capacity peaks were relatively broad and skewed at the high-temperature shoulder, and the maximum excess molar heat capacity appeared at temperatures corresponding to 0.58−0.61 of the heat absorption, an independent proof of the bimolecular nature of the folding/unfolding

reaction (*38*).

The relatively low total peptide concentrations (1 mg/mL or less) precluded precise determination of the absolute partial heat capacity. Therefore, the traces shown in Figure 6 were shifted on the *y*-axis so that the heat capacity of the unfolded state corresponded to the heat capacity of the completely unfolded state calculated from the amino acid composition (*39*).[2] The mean absolute heat capacity of peptide A at 25 °C was 1.67 ± 0.2 J K^{-1} g^{-1}, typical of a small well-packed protein. The temperature dependence of the absolute C_p of A_2 had a slope of (9.2 ± 3.1) × 10^{-3} J K^{-2} g^{-1} (22 measurements) and was apparently independent of pH and C_{tot}. The value was higher than that of an average monomeric compact protein.

It is difficult to precisely measure ΔC_p from DSC scans when the transition takes place in a broad temperature interval and the unfolding enthalpy is relatively small, as it was the case for peptide A. Linear extrapolation of the pre- and post-transition traces to the transition zone gave $\Delta C_p(T_m)$ = (0.8 ± 0.6) kJ K^{-1} mol^{-1} (mean of 22 experiments). At 25 °C, the mean ΔC_p was estimated from the difference between the measured C_p of the folded state and the calculated C_p of the completely unfolded state: ΔC_p(25 °C) = (1.86 ± 0.45) kJ K^{-1} mol^{-1} (mean of 22 experiments). Both estimates were apparently independent of pH and C_{tot}. Hence, $\Delta C_p(T_m)$ and ΔC_p(25 °C) differed by −1 kJ K^{-1} mol^{-1} and, therefore, ΔC_p was not constant. However, a change of ΔC_p by −1 kJ K^{-1} mol^{-1} from 25 to 75 °C (the average T_m was 75 °C) changed the excess unfolding enthalpy by only 20−25 kJ mol^{-1}. This was within the limit of error of the experimentally determined enthalpy change (Table 2).

Not only was the shape of the DSC trace in accord with a two-state transition but also the fitting of the excess heat capacity for an *n*-mer (eq 10) gave n = 2.18 ± 0.15, in agreement with a monomer−dimer folding equilibrium. Representative examples of these fits are shown in the inset of Figure 6. The three methods to calculate ΔH_{cal}, ΔH_{vH}, and ΔH_{fit} gave consistent results (Table 2 and Methods). $\Delta H_{cal}/\Delta H_{vH}$ was 0.94 ± 0.04, again in support of a two-state transition.

Figure 7 shows the entire set of enthalpy changes in the pH range 3.5−4.7 as a function of T_m or $T_{m0.5}$. Values outside this pH range were not considered because the pre- and/or post-transition baselines were less accurate. ΔC_p of unfolding from DSC and CD agreed well. The mean value from all measurements was ΔC_p = 1.98 ± 0.60 kJ mol^{-1} K^{-1}. Enthalpy changes from CD unfolding were slightly larger than those from DSC.

Stability Curves. Values of ΔH_m and T_m were used to calculate the unfolding free energy, ΔG^{unf}, as a function of temperature, that is, the stability curve of the dimer A_2. Curves for the data sets obtained at pH 4.7 and 3.5 (Tables 1 and 2) are shown in Figure 8 and were calculated with the help of the Gibbs−Helmholtz equation adapted to a monomer−dimer equilibrium (*16*, *34*):

[2] This calculation may not be very precise because the ratio of protonated to deprotonated carboxylic groups changed with pH. However, the error could not be large as ionization contributes little to the overall heat capacity function (*44*).

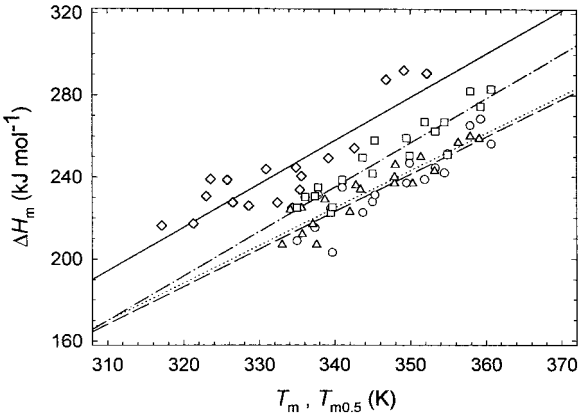

FIGURE 7: Van't Hoff analysis of CD and DSC thermal unfolding experiments performed in the pH range 3.5−4.7 (data from Tables 1 and 2): diamonds and solid line, ΔH_m and T_m from CD unfolding experiments, ΔC_p = 2.1 kJ mol^{-1} K^{-1}; circles and dotted line, ΔH_{cal} and T_m from DSC, ΔC_p = 1.83 kJ mol^{-1} K^{-1}; triangles and dashed line, ΔH_{fit} and $T_{m0.5}$ from DSC, ΔC_p = 1.83 kJ mol^{-1} K^{-1}; squares and dash-dotted line, ΔH_{vH} and T_m from DSC, ΔC_p = 2.14 kJ mol^{-1} K^{-1}. See Methods for how ΔH_m, ΔH_{cal}, ΔH_{fit}, T_m and $T_{m0.5}$ were obtained. The mean ΔC_p from all experiments was 1.98 ± 0.60 kJ mol^{-1} K^{-1}. This value was used to calculate the stability curves in Figures 8, 9, and 11.

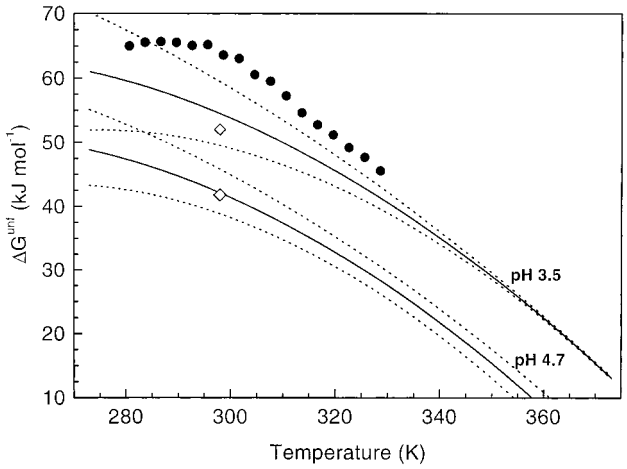

FIGURE 8: Temperature dependence of the free energy of unfolding, ΔG_{unf}, of leucine zipper A_2. The upper curve is for pH 3.5 and the lower curve for pH 4.7. The curves were calculated according to eq 15 with ΔC_P = 1.98 kJ mol^{-1} K^{-1} and using all ΔH_m-T_m pairs from the experiments performed with peptide concentrations above 300 μM at pH 3.5 and 4.7, respectively (Tables 1 and 2). The dashed envelopes were calculated for a 30% error of ΔC_p: filled circles, ΔG^{unf} obtained by the linear extrapolation method (*35*) from thermal unfolding in the presence of increasing amounts of GdmCl; open diamonds, ΔG^{unf} calculated from rate constants (Figure 4) according to $\Delta G^{unf} = -RT \ln(2k_{off}/k_{on})$.

$$\Delta G^{unf}(T) = \Delta H_m\left(1 - \frac{T}{T_m}\right) + \Delta C_p\left[T - T_m - T\ln\left(\frac{T}{T_m}\right)\right] - RT\ln[K_{unf}(T_m)] \quad (15)$$

$K_{unf}(T_m) = C_{tot}$ for a monomer−homodimer equilibrium. The open diamonds in Figure 8 show that the kinetically determined ΔG^{unf} was within the limit of error of ΔG^{unf} from equilibrium thermodynamics.

To demonstrate the high stability of protonated A_2 by an independent experiment, we also measured CD unfolding curves in the presence of increasing amounts of GdmCl at

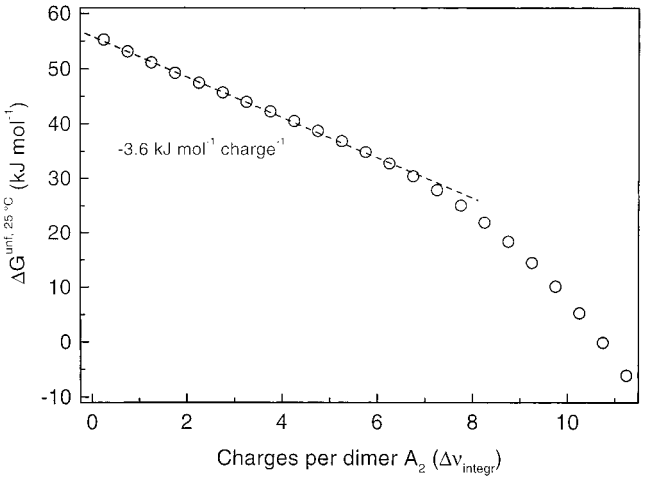

FIGURE 9: Change of the free energy of unfolding at 25 °C with the number of negative charges introduced on deprotonation of leucine zipper A_2. ΔG^{unf} decreases linearly by -3.6 kJ mol^{-1} charge^{-1} up to 6−7 charges per A_2. ΔG^{unf} was calculated with eq 15 in steps of 0.5 charges. The relationship between the number of charges on A_2 and K_{unf} is defined by eq 7 and depicted as $\Delta\nu_{integr}$ versus pH in the inset of Figure 2.

pH 3.5. ΔG^{unf} was obtained by the linear extrapolation method (*35*) between 5 and 55 °C (not shown). ΔG^{unf} from GdmCl-induced unfolding was slightly higher than ΔG^{unf} from thermal unfolding in the absence of denaturant (filled circles in Figure 8).

Electrostatic Repulsion Between g and e Positions. The sharp drop in $[\theta]_{222}$ above pH 5 reflects increasing electrostatic repulsion (Figure 2). To demonstrate the energetic contribution of electrostatic repulsion, we plotted ΔG^{unf}(25 °C) against the number of charges on folded A_2 (Figure 9). The net decrease in ΔG^{unf} per charge was linear for the initial 6−7 charges and thereafter decreased more steeply. The slope of the initial decrease is -3.6 kJ mol^{-1} charge^{-1}. If kinetic and equilibrium experiments concur, this slope should be equivalent to the slope defined by eq 14. The agreement is very good: $-RT(m_{off} - m_{on}) = -3$ kJ mol^{-1} charge^{-1} (data from legend to Figure 4).

DISCUSSION

Two-State Folding Mechanism. Folding of an oligomeric protein can occur in two ways. The subunits can fold first and then associate to the native protein. Alternatively, if the folded conformation of the subunit in isolation is unstable, folding and association are coupled. Coiled coils and leucine zippers fold in the latter way because their component peptide chains lack tertiary structure when dissociated. We have performed a combined kinetic and thermodynamic analysis of a short model leucine zipper formed by the pH-dependent association of two 30-residue peptide chains. Rapid mixing and thermal unfolding experiments supported a simple two-state folding reaction from unordered monomer to ordered dimer. The stopped-flow traces were well-described by eq 3 for a two-state reaction. ΔG^{unf} determined by equilibrium thermal unfolding (eq 15) was the same within error as that calculated from kinetics (eq 14). Enthalpy changes from calorimetry (Table 2) were very similar to van't Hoff enthalpy changes from CD unfolding curves (Table 1). Finally, a rigorous analysis of the DSC traces by three different methods and analysis of the CD unfolding curves agreed with a two-state model.

Is such a simple mechanism compatible with a coupled folding/association reaction? Obviously, two unordered peptide chains cannot associate and fold in a single reaction step. Indeed, folding of some leucine zippers can exhibit two or more steps under some conditions (*25*, *27*), and folding of the extended coiled coil of tropomyosin is at least biphasic (*24*). However, a two-state folding mechanism is not an all-or-none event encompassing only a disordered monomer and a folded dimer. Rather, in a two-state mechanism all molecular conformations can be divided into two groups separated by a high-energy barrier, that is, between chiefly disordered monomer and chiefly folded native dimer. Folding appears to be two-state if intermediates are very short-lived and/or are present at very low concentration (*26*, *29*, *45*).

Folding in the Absence of Interhelical Electrostatic Repulsion is Diffusion-Limited. Measured rate constants (k_{on}) of leucine zipper folding range from 10^5 M^{-1} s^{-1} (*26*) to 7×10^7 M^{-1} s^{-1} (*29*). The latter value pertains to the heterodimeric model leucine zipper AB, which is stabilized at low salt concentrations by electrostatic interactions between Glu in *e* and *g* positions of the A chain and Lys in the same positions of the opposite B chain (Figure 1). The association rate constant for the heterodimer AB increased with decreasing salt concentration (decreasing ionic strength) in support of a dominant contribution of electrostatic interactions to folding. When extrapolated to zero ionic strength, folding of the heterodimer AB was diffusion-limited. Other leucine zippers studied to date and containing no or very few interhelical electrostatic bonds fold 100−1000 more slowly than AB at low ionic strength. One may ask if very rapid folding is possible without electrostatic steering. Since peptides A and B all fold to the homodimers A_2 and B_2 at low and high pH, respectively, folding in the absence of electrostatic effects can be studied by protonation of peptide A or by deprotonation of peptide B. We have concentrated on peptide A because thermal unfolding of peptide B at pH >10, where it is uncharged, was irreversible, and a combined thermodynamic and kinetic study was not possible (E.D. unpublished results). The maximum rate constant of folding of two protonated peptides A was $k_{on} = 3 \times 10^8$ M^{-1} s^{-1}. This is close to the diffusion limit estimated to be 5×10^9 M^{-1} s^{-1} using the von Smoluchowski equation (*46*, *47*).[3]

Why does uncharged A_2 fold so fast? In diffusion-limited folding the highest-energy barrier is overcome in the formation of the initial collision complex since almost all collisions are successful. Folding to the final coiled coil is along a "down-hill" energy landscape. Formation of the helices cannot be rate-limiting since α-helices fold orders of magnitude faster than the time necessary for diffusion-limited association (*48*−*50*). Also, preformation of helical structure in monomeric peptide A can be excluded (*28*). Therefore, one may speculate that the transition state is close in energy to the collisional complex and that it is not yet well-structured. This idea is in line with the a nucleation−condensation pathway (*51*) or a molecular collapse model (*52*, *53*). Both visualize a folding pathway without accretion

[3] The diffusion-limited rate was estimated from $k_{diff} = 16\pi r_A D_A N 10^{-3}$ where r_A is the reaction radius (in cm) of peptide A, D_A is the diffusion coefficient (in cm^2 s^{-1}), and N is Avogadro's number. $r_A = 1.2 \times 10^{-7}$ cm was estimated for a globular, hydrated molecule ($M_r = 3468$, 0.57 g of H_2O/g of peptide) and $D_A = 1.8 \times 10^{-6}$ cm^2 s^{-1} from $D_A = k_B T/6\pi\eta r_A$ where η is the viscosity and k_B is the Boltzmann constant.

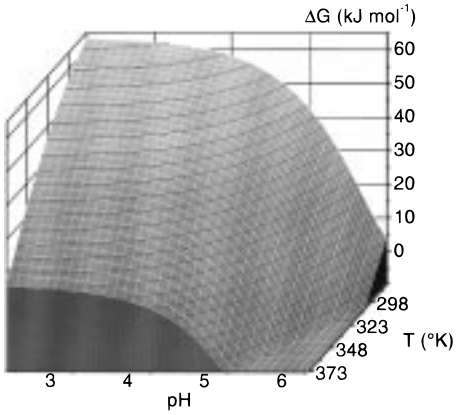

FIGURE 10: Temperature−pH stability surface of leucine zipper A_2. The surface was calculated using the CD data for pH = 2.75−6.5 and T = 273−373 K with the help of eq 15. $\Delta H_m(T_m)$ was obtained from the regression line in Figure 7 and T_m(pH) from panel A of Figure 5.

of stable elements of structure as a prerequisite for successful folding. Perhaps it is more adequate to imagine a large ensemble of energetically similar transition states with little conformational restrictions from which the "downhill" folding to the coiled coil initiates (*54*, *55*).

Since the uncharged leucine zipper A_2 is mainly stabilized by hydrophobic interactions at the dimer interface and has no contributions from favorable electrostatic bonds, its structure may be less geometrically constrained than that of the electrostatically stabilized AB dimer. This may also have contributed to the very rapid folding of A_2 since formation of precisely oriented polar interactions is an inherently difficult step. Indeed, AB folds 10 times more slowly than A_2 at 0.1 M ionic strength where folding of A_2 was analyzed (*29*). In the Arc repressor protein dimer, a buried network of salt bridges slows folding, and their mutation to hydrophobic residues increases the folding rate to the diffusion limit (*56*).

There is another noteworthy difference between the folding/unfolding kinetics of A_2 and AB. Electrostatic attraction increases the rate of folding of AB but has only a very minor influence on the rate of dissociation and unfolding of AB. This contrasts to the effect of charge−charge repulsion on folding/unfolding of A_2 seen here. Increasing the pH decreased k_{on} and increased k_{off} to the same extent (slopes in Figure 4). Hence, one may conclude that electrostatic repulsion plays a more general role in folding/unfolding than electrostatic attraction. This explains in kinetic terms what had been observed in equilibrium thermodynamics for leucine zippers (*12*−*18*, *57*−*60*) and for globular proteins in general (*61*, *62*): opposing charges are always destabilizing while potential attractive charges may or may not contribute to stability.

Uncharged Dimer A_2 is More Stable than Can Be Accounted for by the Loss of Charge−Charge Repulsion Alone. Figure 10 shows the pH-temperature-stability surface of leucine zipper A_2. The figure represents the extended set of thermodynamic data obtained for the folding of A_2 over a large range of pH and temperature. The steep descent of the surface reflects the large repulsive destabilization per charge, which is mirrored by an equally large decrease of k_{on} and increase of k_{off}. Interestingly, uncharged, protonated A_2 is more stable than the electrostatically stabilized leucine zipper AB. ΔG^{unf} of fully protonated A_2 is at least 55 kJ mol^{-1}, which is the value at pH 3.5 and 25 °C obtained from the stability curve in Figure 8. Leucine zipper AB has ΔG^{unf} = 43 kJ mol^{-1} (22 mM ionic strength, pH 7, 25 °C; ref 16). At low salt concentration electrostatic attraction between an interhelical Glu-Lys pair in the center of a disulfide-linked leucine zipper is worth about 2 kJ mol^{-1} (*18*). AB has six potential attractive $e-g$ pairs not considering the e and g positions next to each end of the coiled coil. The ends of a coiled coil are frayed, and electrostatic interactions cannot be strong (*63*). Subtracting the free energy of six Glu-Lys pairs from ΔG^{unf} of AB leaves ΔG^{unf} = 31 kJ mol^{-1}, which is about 24 kJ mol^{-1} less than ΔG^{unf} of uncharged A_2. This is surprising since A_2 and AB have identical residues in the a and d positions of the hydrophobic core. The much higher stability of A_2 may be explained if one considers that the protonated glutamic acid side chain has the properties of a nonpolar residue. It is significantly less polar than the uncharged side chain of Gln.[4] Mutational studies in a disulfide-linked model coiled coil by Hodges and co-workers showed that mutation of e and g positions increases stability in the following order: deprotonated Glu < Gln < protonated Glu (*64*).

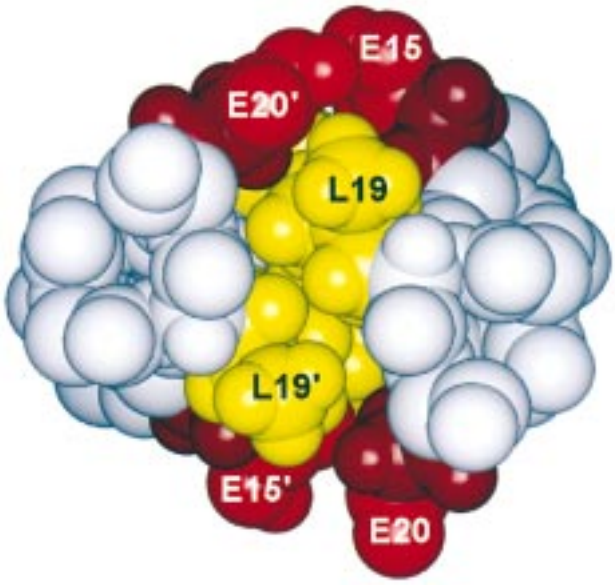

FIGURE 11: Space-filling model of a cross-section through fully protonated A_2. The view is perpendicular to the long axis of the coiled coil. The two helices are in light gray, leucines in d positions are in yellow, and protonated glutamic acid residues in e positions are in red; side chain methylene groups of Glu are colored in a darker hue. The structure was modeled on that of the leucine zipper domain of GCN4, minimized, and subjected to a 100 ps molecular dynamics simulation at 298 K (see Methods). No significant deviations from the minimized starting structure were observed during the 100 ps simulation (backbone rms deviation = 0.46 ± 0.06 Å, heavy atom rms deviations = 0.78 ± 0.09 Å).

Figure 11 shows a cross-section through the leucine zipper A_2 modeled on the crystal structure of the GCN4 leucine zipper domain (*19*). The figure illustrates how the side chains of uncharged Glu in e positions can fold back and oppose the side chains in d positions. (The same applies to g and a

[4] The dipole moment of protonated acetic acid in the gas phase is 1.74 and that of acetamide is 3.76 D (Handbook of Physics and Chemistry, 44th edition, Chemical Rubber Publishing Co., Cleveland, OH, 1962).

positions.) Hence, the difference in ΔG^{unf} between A_2 and AB can be rationalized if one assumes that protonation of Glu strengthens the hydrophobic core. A single methylene group adds approximately 2 kJ mol^{-1} to ΔG^{unf}, a figure obtained by Leu/Ala mutations in engineered leucine zippers (*16*, *65*). Hence, all other things being equal, the extra 24 kJ mol^{-1} of stabilizing free energy of A_2 compared to AB can be explained by roughly 12 extra methylene groups contributing to the hydrophobic core. Obviously, the protonated Glu side chains are not optimally packed to form a tight hydrophobic core together with the *a* and *d* side chains. Otherwise, the expected stabilization would be even larger since burying a methylene group in the optimized hydrophobic interior of a protein contributes about 6 kJ mol^{-1} (*66*). In support of a strengthened hydrophobic core we note that the heat capacity change of 2 kJ mol^{-1} K^{-1} for A_2 is about double ΔC_P for the folding of the 33-residue leucine zipper domain of GCN4 (*67*, *68*). Calculation of ΔC_P from the water-accessible surface buried in the A_2 model (Figure 11) yields 1.4 kJ mol^{-1} K^{-1}. In the calculation protonated Glu was treated as a polar residue that does not contribute to the buried surface (see Methods). The difference between measured and calculated ΔC_P gives indirect support to the formation of a more extended hydrophobic core in protonated A_2.

Surprisingly, ΔC_P of electrostatically stabilized AB is 4.2 kJ mol^{-1} K^{-1} (*16*), twice ΔC_P of A_2. It has been shown also for other leucine zippers that ΔC_P increases with the number of interhelical ionic bonds (*13*, *18*). Possibly interhelical electrostatic interactions and other geometrical constraints increase ΔC_P above the magnitude expected on the basis of surface burial alone. Experiments as well as theoretical considerations indicate that ΔC_P originates from changes in the degree of surface hydration in the unfolded and the folded molecule and to a lesser extent also from changes in molecular vibrations (*39*, *44*, *69*−*71*). A coiled coil with many interhelical polar bonds seems to display more surface hydration and more restrictions in the vibrational modes of polar groups and of bound water molecules.

ACKNOWLEDGMENT

We thank Antonio Baici for assistance in the stopped-flow experiments and Stefan Klauser for help in peptide synthesis.

REFERENCES

1. Lupas, A. (1996) *Trends Biochem. Sci. 21,* 375−382.
2. Crick, F. H. C. (1953) *Acta Crystallogr. 6,* 689−697.
3. Cohen, C., and Parry, D. A. D. (1990) *Proteins 7,* 1−15.
4. Hope, I. A., and Struhl, K. (1987) *EMBO J. 6,* 2781−2784.
5. Landschulz, W. H., Johnson, P. F., and McKnight, S. L. (1988) *Science 240,* 1759−1764.
6. Hurst, H. C. (1996) *Leucine Zippers: Transcription factors*, Academic Press, London.
7. Hodges, R. S., Semchuk, P. D., Taneja, A. K., Kay, C. M., Parker, J. M. R., and Mant, C. T. (1988) *Pept. Res. 1,* 19−30.
8. Bryson, J. W., Betz, S. F., Lu, H. S., Suich, D. J., Zhou, H. X. X., O'Neil, K. T., and DeGrado, W. F. (1995) *Science 270,* 935−941.
9. Alber, T. (1992) *Curr. Opin. Genet. Dev. 2,* 205−210.
10. Vinson, C. R., Hai, T., and Boyd, S. M. (1993) *Genes Dev. 7,* 1047−1058.
11. Graddis, T. J., Myszka, D. G., and Chaiken, I. M. (1993) *Biochemistry 32,* 12664−12671.
12. O'Shea, E. K., Lumb, K. J., and Kim, P. S. (1993) *Curr. Biol. 3,* 658−667.
13. Krylov, D., Mikhailenko, I., and Vinson, C. (1994) *EMBO J. 13,* 2849−2861.
14. Zhou, N. E., Kay, C. M., and Hodges, R. S. (1994) *J. Mol. Biol. 237,* 500−512.
15. Kohn, W. D., Monera, O. D., Kay, C. M., and Hodges, R. S. (1995) *J. Biol. Chem. 270,* 25495−25506.
16. Jelesarov, I., and Bosshard, H. R. (1996) *J. Mol. Biol. 263,* 344−358.
17. Kohn, W. D., Kay, C. M., and Hodges, R. S. (1997) *J. Mol. Biol. 267,* 1039−1052.
18. Krylov, D., Barchi, J., and Vinson, C. (1998) *J. Mol. Biol. 279,* 959−972.
19. O'Shea, E. K., Klemm, J. D., Kim, P. S., and Alber, T. (1991) *Science 254,* 539−544.
20. Ellenberger, T. (1994) *Curr. Opin. Struct. Biol. 4,* 12−21.
21. O'Shea, E. K., Rutkowski, R., Stafford, W. F., III, and Kim, P. S. (1989) *Science 245,* 646−648.
22. Lamb, P., and McKnight, S. L. (1991) *Trends Biochem. Sci. 16,* 417−422.
23. Baxevanis, A. D., and Vinson, C. R. (1993) *Curr. Opin. Genet. Dev. 3,* 278−285.
24. Ozeki, S., Kato, T., Holtzer, M. E., and Holtzer, A. (1991) *Biopolymers 31,* 957−966.
25. Wendt, H., Baici, A., and Bosshard, H. R. (1994) *J. Am. Chem. Soc. 116,* 6973−6974.
26. Zitzewitz, J. A., Bilsel, O., Luo, J. B., Jones, B. E., and Matthews, C. R. (1995) *Biochemistry 34,* 12812−12819.
27. Wendt, H., Berger, C., Baici, A., Thomas, R. M., and Bosshard, H. R. (1995) *Biochemistry 34,* 4097−4107.
28. Sosnick, T. R., Jackson, S., Wilk, R. R., Englander, S. W., and Degrado, W. F. (1996) *Proteins 24,* 427−432.
29. Wendt, H., Leder, L., Härmä, H., Jelesarov, I., Baici, A., and Bosshard, H. R. (1997) *Biochemistry 36,* 204−213.
30. Jelesarov, I., Dürr, E., Thomas, R. M., and Bosshard, H. R. (1998) *Biochemistry 37,* 7539−7550.
31. Edelhoch, H. (1967) *Biochemistry 6,* 1948−1954.
32. Gill, S. C., and von Hippel, P. (1989) *Anal. Biochem. 182,* 319−326.
33. Milla, M. E., and Sauer, R. T. (1994) *Biochemistry 33,* 1125−1133.
34. Marky, L. A., and Breslauer, K. J. (1987) *Biopolymers 26,* 1601−1620.
35. Pace, C. N. (1986) *Methods Enzymol. 131,* 266−280.
36. Wyman, J., Jr. (1964) *Adv. Protein Chem. 19,* 223−244.
37. Plotnikov, V. V., Brandts, J. M., Lin, L. N., and Brandts, J. F. (1997) *Anal. Biochem. 250,* 237−244.
38. Privalov, P. L., and Pothekin, S. A. (1986) *Methods Enzymol. 131,* 4−51.
39. Makhatadze, G. I., and Privalov, P. L. (1995) *Adv. Protein Chem. 47,* 307−425.
40. Ellenberger, T. E., Brandl, C. J., Struhl, K., and Harrison, S. C. (1992) *Cell 71,* 1223−1237.
41. Lumb, K. J., and Kim, P. S. (1995) *Biochemistry 34,* 8642−8648.
42. Junius, F. K., Mackay, J. P., Bubb, W. A., Jensen, S. A., Weiss, A. S., and King, G. F. (1995) *Biochemistry 34,* 6164−6174.
43. Zeng, X., Herndon, A. M., and Hu, J. C. (1997) *Proc. Natl. Acad. Sci. U.S.A. 94,* 3673−3678.
44. Gomez, J., Hilser, V. J., Xie, D., and Freire, E. (1995) *Proteins 22,* 404−412.
45. Qian, H. (1994) *Biophys. J. 67,* 349−355.
46. von Smolukowski, M. (1917) *Z. Phys. Chem. 92,* 129−168.
47. Moser, C. C., and Dutton, P. L. (1988) *Biochemistry 27,* 2450−2461.
48. Schwarz, G. (1965) *J. Mol. Biol. 11,* 64−77.
49. Hammes, G. G., and Roberts, P. B. (1969) *J. Am. Chem. Soc. 91,* 1812−1816.
50. Williams, S., Causgrove, T. P., Gilmanshin, R., Fang, K. S., Callender, R. H., Woodruff, W. H., and Dyer, R. B. (1996) *Biochemistry 35,* 691−697.
51. Fersht, A. R. (1995) *Proc. Natl. Acad. Sci. U.S.A. 92,* 10869−10873.

52. Dill, K. (1985) *Biochemistry 24,* 1501−1504.
53. Sosnick, T. R., Shtilerman, M. D., Mayne, L., and Englander, S. W. (1997) *Proc. Natl. Acad. Sci. U.S.A. 94,* 8545−8550.
54. Dill, K. A., and Chan, H. S. (1997) *Nat. Struct. Biol. 4,* 10−19.
55. Baldwin, R. L. (1997) *Nat. Struct. Biol. 4,* 965−966.
56. Waldburger, C. D., Jonsson, T., and Sauer, R. T. (1996) *Proc. Natl. Acad. Sci. U.S.A. 93,* 2629−2634.
57. Lumb, K. J., and Kim, P. S. (1995) *Science 268,* 436−439.
58. Lumb, K. J., and Kim, P. S. (1996) *Science 271,* 1137−1138.
59. Lavigne, P., Kondejewski, L. H., Houston, M. E., Jr., Sönnichsen, F. D., Lix, B., Sykes, B. D., Hodges, R. S., and Kay, C. M. (1995) *J. Mol. Biol. 254,* 505−520.
60. Lavigne, P., Sönnichsen, F. D., Kay, C. M., and Hodges, R. S. (1996) *Science 271,* 1136−1137.
61. Perutz, M. F. (1978) *Science 201,* 1187−1191.
62. Honig, B., and Nicholls, A. (1995) *Science 268,* 1144−1149.
63. Zhang, L., and Hermans, J. (1993) *Proteins 16,* 384−392.
64. Kohn, W. D., Kay, C. M., and Hodges, R. S. (1995) *Protein Sci. 4,* 237−250.
65. Zhou, N. E., Kay, C. M., and Hodges, R. S. (1992) *Biochemistry 31,* 5739−5746.
66. Matthews, B. W. (1993) *Annu. Rev. Biochem. 62,* 139−160.
67. Thompson, K. S., Vinson, C. R., and Freire, E. (1993) *Biochemistry 32,* 5491−5496.
68. Kenar, K. T., Garcia-Moreno, B., and Freire, E. (1995) *Protein Sci. 4,* 1934−1938.
69. Sturtevant, J. M. (1977) *Proc. Natl. Acad. Sci. U.S.A. 74,* 2236−2240.
70. Murphy, K. P., and Freire, E. (1992) *Adv. Protein Chem. 43,* 313−361.
71. Spolar, R. S., Livingstone, J. R., and Record, M. T., Jr. (1992) *Biochemistry 31,* 3947−3955.
72. Makhatadze, G. I., and Privaolv, P. L. (1993) *J. Mol. Biol. 232,* 639−659.

BI981891E